2019

Flexural design of GFRP bar reinforced concrete beams: An appraisal of code recommendations

Zein Saleh
University of Wollongong, zs492@uowmail.edu.au

Matthew Goldston
University of Wollongong, mwg278@uowmail.edu.au

Alex M. Remennikov
University of Wollongong, alexrem@uow.edu.au

M Neaz Sheikh
University of Wollongong, msheikh@uow.edu.au

Flexural design of GFRP bar reinforced concrete beams: An appraisal of code recommendations

Abstract
In this paper, two design codes for the flexural design of Fibre Reinforced Polymer (FRP) bar reinforced concrete beams have been reviewed and compared with the results of the experimental investigations of eight GFRP (Glass Fibre-Reinforced Polymer) bar reinforced concrete (GFRP-RC) beams. It has been demonstrated that experimentally determined load carrying capacities, maximum deflections and energy absorbing capacities have been over-predicted by the relevant code recommendations for the under-reinforced and balanced GFRP-RC beams while being under-predicted for the over-reinforced GFRP-RC beams. This paper will provide a better understanding on the design methods in the two codes to the designers and rational suggestions for further improvements to the code design recommendations.

Disciplines
Engineering | Science and Technology Studies

Publication Details
Saleh, Z., Goldston, M., Remennikov, A. M. & Sheikh, M. (2019). Flexural design of GFRP bar reinforced concrete beams: An appraisal of code recommendations. Journal of Building Engineering, 25 100794-1-100794-10.

Flexural Design of GFRP Bar Reinforced Concrete Beams: An Appraisal of Code Recommendations

Zein Saleh[1], Matthew Goldston[2], Alex M. Remennikov[3], and M. Neaz Sheikh[4*]

[1]Ph.D. Candidate, School of Civil, Mining and Environmental Engineering, University of Wollongong, Wollongong, NSW 2522, Australia. E-mail: zs492@uowmail.edu.au

[2]PhD. School of Civil, Mining and Environmental Engineering, University of Wollongong, Wollongong, NSW 2522, Australia. E-mail: mwg278@uowmail.edu.au

[3]Professor, School of Civil, Mining and Environmental Engineering, University of Wollongong, Wollongong, NSW 2522, Australia. E-mail: alexrem@uow.edu.au

[4]Associate Professor, School of Civil, Mining and Environmental Engineering, University of Wollongong, Wollongong, NSW 2522, Australia (corresponding author). E-mail: msheikh@uow.edu.au

[*]**Correspondence**:

M. Neaz Sheikh

School of Civil, Mining & Environmental Engineering

University of Wollongong, Australia

E-mail: msheikh@uow.edu.au

Telephone: + 61 2 4221 3009

Facsimiles: + 61 2 4221 3238

----

* Corresponding author

Flexural Design of GFRP Bar Reinforced Concrete Beams: An Appraisal of Code Recommendations

Zein Saleh[1], Matthew Goldston[2], Alex M. Remennikov[3], and M. Neaz Sheikh[4*]

ABSTRACT

In this paper, two design codes for the flexural design of Fibre Reinforced Polymer (FRP) bar reinforced concrete beams have been reviewed and compared with the results of the experimental investigations of eight GFRP (Glass Fibre-Reinforced Polymer) bar reinforced concrete (GFRP-RC) beams. It has been demonstrated that experimentally determined load carrying capacities, maximum deflections and energy absorbing capacities have been over-predicted by the relevant code recommendations for the under-reinforced and balanced GFRP-RC beams while being under-predicted for the over-reinforced GFRP-RC beams. This paper will provide a better understanding on the design methods in the two codes to the designers and rational suggestions for further improvements to the code design recommendations.

Keywords: GFRP, Reinforced Concrete, Beam, Flexure, Design Recommendation

1. Introduction

Traditional Reinforced Concrete (RC) structures exposed to highly aggressive environments are susceptible to corrosion of the steel reinforcement, resulting in the loss of durability and serviceability. To counteract this problem, Fibre Reinforced Polymer (FRP), as a non-corrosive material, can substitute traditional steel reinforcement in RC structures. The FRP is a composite and anisotropic material containing fibres embedded within a polymeric matrix. The advantages of FRP include high strength to weight ratio, non-conductivity, electromagnetic neutrality, and non-corrosiveness. Although FRP is currently expensive compared to steel reinforcement, the low maintenance costs over the service life of the structure may make FRP a feasible option. The FRP reinforcement can be used in the form of plates or sheets as external reinforcement [1-3] or as the confinement for RC columns [4, 5]. The FRP bars have been recently used as the internal reinforcement in concrete beams [6, 7]. The most popular types of FRP bar reinforcement include Aramid FRP (AFRP), Glass FRP (GFRP), and Carbon FRP (CFRP). Among these FRP reinforcement bar types, the GFRP bars are the most popular due to their abundance and relatively low cost. The behaviour of GFRP bar reinforced concrete beams was investigated in recent years [8-21]. It was found that increasing the FRP reinforcement ratio in GFRP bar Reinforced Concrete (GFRP-RC) beams constructed with normal strength concrete resulted in a decrease in the maximum midspan deflection and the crack width [20]. Moreover, GFRP-RC beams constructed with high strength concrete provided improved load carrying capacity and reduced deflection compared to GFRP-RC beams constructed with normal strength concrete [22]. Furthermore, the type of GFRP bar (sand coated, helically grooved, or deformed) and the bar diameter influenced the bond strength and crack width of GFRP bars with concrete [23].

Recent research investigations have led to the development of design codes for FRP bars reinforced concrete (FRP-RC) structures including “Guide for the Design and Construction of Structural Concrete Reinforced with Fiber-Reinforced Polymer (FRP) Bars” (ACI [24]) and “Design and construction of building structures with fibre-reinforced polymers” (CSA [25]). However, the code recommendations for the flexural design of GFRP-RC beams have not been adequately compared with the experimental investigations results. In this paper, design code recommendations in ACI [24] and CSA [25] for the flexural design of FRP-RC beams are reviewed. Experimental investigation results of eight GFRP-RC beams tested under flexural load have been presented. Recommendations in ACI [24] and CSA [25] for the calculation of nominal loads, midspan deflections at nominal loads, and Energy Absorption Capacities (EAC) of GRRP-RC beams are critically compared with the experimental results.

2. Review of design recommendations for FRP-RC beams

Mechanical and physical properties of FRP bars are significantly different than those of steel reinforcement bars. FRP is a linear elastic material whereas steel reinforcement is ductile (Figure 1). The tensile strength of GFRP and CFRP can vary from 483 MPa to 1600 MPa and 600 MPa to 3690 MPa respectively, compared to 483 MPa to 690 MPa for steel reinforcement ACI [24]). However, the elastic modulus of FRP, especially GFRP, is considerably lower than the elastic modulus of steel reinforcement (35-51 GPa for GFRP and 200 GPa for Steel) (ACI [24]). Table 1 summarises the typical material properties of FRP bars and steel bars according to ACI [24]. Significant differences in the behaviour of FRP reinforced and traditional steel bar Reinforced Concrete (Steel-RC) beams have led to the development of design recommendations for FRP-RC beams [19-23]. According to the FRP design recommendations, the preferred failure mode of FRP-RC beams was concrete crushing, as the beam experiences some form of "ductility" and plastic behaviour before failure. Rupture of the FRP bars in tension can be catastrophic and may occur without any warning and should be avoided (as FRP is a linear-elastic material). Hence, the design philosophy of FRP-RC beams differs from that of traditional Steel-RC beams. For traditional Steel-RC beams, yielding of steel before reaching the moment capacity is essential, as it provides ductility and warning of failure. For FRP-RC structures, failure due to concrete crushing is preferred since it provides pseudo-ductile failure and warnings before the collapse of the structure. The following sub-sections (sub-sections 2.1 and 2.2) provide a review of the current FRP design code recommendations (ACI [24] and CSA [25]) for FRP-RC beams in terms of the calculation of nominal flexural capacity (design for flexure) and midspan deflection.

2.1 *American Concrete Institute Guide (ACI [20])*

The American Concrete Institute (ACI) Committee 440 developed a guide for the design of concrete structures with FRP Bars (ACI [24]). The ACI [24] states that the flexural capacity of FRP-RC beams can be calculated similarly to that of Steel-RC beams. The ACI [24] does not recommend the use of FRP reinforcement in compression for flexural members due to the lower compressive strength compared to the tensile strength of FRP bars. Hence, the contribution of the FRP bars in compression for FRP-RC flexural members was neglected in the design process.

2.1.1 *Design for flexure*

The recommended failure mode of an FRP-RC member was by concrete crushing (over-reinforced section) which was preferred over the failure due to rupture of FRP bars (under-reinforced section). This was particularly because if the FRP bars reach the rupture strain (ε_{fu}), the failure will be sudden and non-ductile, unlike concrete crushing. For FRP-RC beam, the balanced reinforcement ratio (ρ_{fb}) can be calculated by Eq. (1).

$$\rho_{fb} = 0.85\beta_1 \frac{f'_c}{f_{fu}} \frac{E_f \varepsilon_{cu}}{E_f \varepsilon_{cu} + f_{fu}} \tag{1}$$

where, f'_c was the compressive strength of concrete at 28 days; E_f was the modulus of elasticity of the FRP bar; ε_{cu} was the ultimate concrete strain (taken as 0.003); f_{fu} was the ultimate tensile strength of the FRP reinforcement; and β_1 was the stress block parameter. The β_1 parameter was calculated by Eq. (2).

$$\beta_1 = \left(0.85 - 0.05\left(\frac{f'_c - 28}{7}\right)\right) \geq 0.65 \tag{2}$$

To ensure the design of an over-reinforced section, the FRP reinforcement ratio (ρ_f) should be 1.4 times larger than the balanced reinforcement ratio $\left(\rho_f > 1.4\rho_{fb}\right)$. The FRP reinforcement ratio can be computed by Eq. (3)

$$\rho_f = A_f / bd \tag{3}$$

where A_f was the area of the FRP tensile reinforcement; b was the width of the beam; and d was the effective depth of the beam.

However, for the FRP bar rupture to occur before concrete crushing, the FRP reinforcement ratio must be less than the balanced reinforcement ratio ($\rho_f < \rho_{fb}$). This is referred to as an under-reinforced design of an FRP-RC section.

For a balanced failure condition, the FRP tensile reinforcement must reach the rupture strain simultaneously with concrete crushing $\left(\varepsilon_f = \varepsilon_{fu} \text{ with } \varepsilon_{cu} = 0.003\right)$, where ε_f is the strain in the FRP bar. The FRP-RC beam was considered balanced when $\rho_{fb} \leq \rho_f \leq 1.4\rho_{fb}$.

For an over-reinforced FRP-RC beam (concrete crushing governs), the rectangular stress block can be used to compute the nominal flexural capacity (M_n) in terms of the FRP reinforcement ratio (Eq. (4)).

$$M_n = \rho_f f_f \left(1 - 0.59 \frac{\rho_f f_f}{f'_c}\right) bd^2 \tag{4}$$

where f_f was the stress in the FRP reinforcement in tension and must be less than or equal to the ultimate tensile strength of the FRP reinforcement (f_{fu}). The f_f can be calculated by Eq. (5).

$$f_f = \sqrt{\frac{\left(E_f \varepsilon_{cu}\right)^2}{4} + \frac{0.85\beta_1 f'_c}{\rho_f} E_f \varepsilon_{cu}} - 0.5 E_f \varepsilon_{cu} \leq f_{fu} \tag{5}$$

For an under-reinforced FRP-RC beam (FRP rupture governs), ACI [24] provides a conservative and simple method for obtaining the nominal flexural capacity (Eq. (6)).

$$M_n = A_f f_{fu} \left(d - \frac{\beta_1 c_b}{2}\right) \tag{6}$$

where c_b was the distance from extreme compression fibre to neutral axis at balanced strain conditions and can be computed by Eq. (7).

$$c_b = \left(\frac{\varepsilon_{cu}}{\varepsilon_{cu} + \varepsilon_{fu}}\right) d \tag{7}$$

According to ACI [24], the nominal flexural strength of a section (M_n) must exceed the factored moment $\left(\frac{M_u}{\emptyset}\right)$ (Eq. (8)).

$$M_n \geq \frac{M_u}{\emptyset} \tag{8}$$

A conservative strength reduction factor ($\emptyset$) in flexure is recommended since FRP-RC beams should have higher reserve strength to account for the lack of ductility. The graph of the strength reduction factor ($\emptyset$) as a function of the reinforcement ratio is presented in Figure 2.

2.1.2 *Calculation of midspan deflection*

The calculation of the midspan deflection in ACI [24] is based on the effective second moment of area, as provided in Eq. (9). The factor γ in Eq. (10) is dependent on the load and boundary conditions and accounts for the length of the uncracked regions of the member and for the change in stiffness in the cracked regions in the FRP-RC beam. The factor γ is presented in Eq. (10) in terms of the applied moment (M_a) and the cracked moment (M_{cr}) provided in Eq. (11). The second moment of area of cracked section (I_{cr}) can be calculated by Eq. (12).

$$I_e = \frac{I_{cr}}{1 - \gamma\left(\frac{M_{cr}}{M_a}\right)^2 \left[1 - \frac{I_{cr}}{I_g}\right]} \leq I_g \tag{9}$$

where M_{cr} was the cracking moment (Eq. (11)), M_a was applied moment where $M_a \geq M_{cr}$, and I_{cr} was second moment of area of the transformed cracked section.

$$\gamma = 1.72 - 0.72\frac{M_{cr}}{M_a} \tag{10}$$

$$M_{cr} = (1.24\, I_g \sqrt{f'_c}) / h \tag{11}$$

$$I_{cr} = \frac{bd^3}{3} k^3 + n_f A_f d^2 (1-k)^2 \tag{12}$$

2.2 *Canadian Design Manual (CSA [25])*

The CSA [25] provides background information in relation to FRP materials, design process for flexure and shear, serviceability limit states, development, anchorage and splicing of reinforcement, placement of reinforcement and constructability and field applications. The CSA [25] recommends that the contribution of the compressive FRP reinforcement and the tensile strength of concrete are ignored.

2.2.1 *Design for flexure*

For the flexural design of FRP-RC beams, CSA [25] recommends concrete crushing failure when the factored resistance of a section is smaller than 1.6 times the effect of the factored load. If the factored resistance of a section is greater than 1.6 times the effect of the factored load, then failure can be initiated by FRP bar rupture. According to CSA [25], the failure due to concrete crushing occurs at $\varepsilon_{cu} = 0.0035$.

In order to calculate the balanced reinforcement ratio of an FRP-RC beam, the concrete compressive force (C) and tensile force (T) are calculated by Eqs. (13) and (14), respectively.

$$C = \alpha \emptyset_c f'_c \beta c_b b \tag{13}$$

$$T = \emptyset_f A_f f_{fu} \tag{14}$$

where f'_c was the compressive strength of concrete at 28 days; A_f was the area of FRP reinforcement; c_b was the depth of the neutral axis; f_{fu} was that ultimate stress of the FRP bar; α and β are stress block parameters, which can be calculated by Eq. (15) and Eq. (16), respectively

$$\alpha = 0.85 - 0.0015 f'_c \geq 0.67 \tag{15}$$

$$\beta = 0.97 - 0.0025 f'_c \geq 0.67 \tag{16}$$

The FRP reinforcement ratio corresponding to a balanced failure (ρ_{fb}) can be calculated by Eq. (17).

$$\rho_{fb} = \alpha\beta \frac{\emptyset_c}{\emptyset_f} \frac{f'_c}{f_{fu}} \left(\frac{\varepsilon_{cu}}{\varepsilon_{cu} + \varepsilon_{fu}} \right) \tag{17}$$

Where the factors $\emptyset_c$ and $\emptyset_f$ are the material resistance factors for concrete and FRP. The factor $\emptyset_c$ was taken as 0.65 for pre-cast concrete and 0.6 for cast in-situ concrete. The factor $\emptyset_f$ was taken as 0.75 for CFRP, GFRP and AFRP.

For the failure due to concrete crushing, equilibrium between the compression and tension forces must apply $(C = T)$. The FRP bars do not rupture in this case. Hence, the stress in the FRP bars was smaller than the ultimate stress $\left(f_f < f_{fu}\right)$. The stress in the FRP bars of an over-reinforced FRP-RC beam can be calculated by Eq. (18).

$$f_f = \frac{1}{2} E_f \varepsilon_{cu} \left[\left(1 + \frac{4\alpha\beta\emptyset_c f'_c}{\rho_f \emptyset_f E_f \varepsilon_{cu}} \right)^{\frac{1}{2}} - 1 \right] \tag{18}$$

Hence, the nominal flexural capacity (M_n) of an over-reinforced FRP-RC beam can be calculated by Eq. (19).

$$M_n = T \left(d - \frac{\beta c_b}{2} \right) \tag{19}$$

where T for an over-reinforced section was calculated by Eq. (20).

$$T = \emptyset_f A_f f_f \tag{20}$$

For the failure to be initiated by FRP rupture $\left(\varepsilon_c < \varepsilon_{cu} \text{ and } \varepsilon_f = \varepsilon_{fu}\right)$, the stress block parameters α and β cannot be used since the strain in concrete at compression was lower than the ultimate compressive strain. Previously, the ISIS (2007) [18] recommended using equivalent stress block parameters for the compressive strength of concrete between 20 MPa and 60 MPa. However, CSA [25] recommends the use of strain compatibility and the relevant stress-strain relationships between concrete and FRP bars. The strain in concrete at compression can be calculated by Eq. (21).

$$\varepsilon_c = c_b \left(\frac{\varepsilon_{fu}}{d - c_b}\right) < \varepsilon_{cu} \tag{21}$$

To avoid failure immediately after cracking, CSA [25] recommends that the nominal flexural capacity should be 1.5 times greater than the cracking moment (Eq. (22)).

$$M_n \geq 1.5M_{cr} \tag{22}$$

where $M_{cr} = f_r I_t / y_t$; f_r is the modulus of rupture of concrete; I_t is the second moment of area of the transformed uncrack sections about its centroidal axis; and y_t is the distance from the centroid of uncracked section to extreme surface in tension.

2.2.2 *Calculation of midspan deflection*

The CSA [25] calculates the midspan deflection of the FRP-RC beam using an effective second moment of area. The effective second moment of area of FRP-RC beams was calculated by Eq. (24). However, if the service load is lower than the cracking load, CSA [25] recommends using the transformed second moment of area, I_t, for calculating the midspan deflection.

$$I_e = \frac{I_t I_{cr}}{I_{cr} + \left(1 - 0.5\left(\frac{M_{cr}}{M_a}\right)^2\right)(I_t - I_{cr})} \tag{24}$$

where I_t is the transformed second moment of area.

3. Experimental program

3.1 ***Preliminary material testing***

Nine sand-coated GFRP bars were tested to measure the ultimate tensile strength (f_{fu}), elastic modulus (E_f), and rupture strain (ε_{fu}). The GFRP bars with three different diameters were tested: 6.35 mm (#2), 9.53 mm (#3) and 12.7 mm (#4). Steel anchors were attached to the end of the specimen using an expansive cement grout, Bristar 100, as recommended in ASTM [24]. Table 2 provides details of the test specimens including, the free length (L), defined as the length between the steel anchors, steel anchor length (L_a), total length of tensile test specimen (L_{tot})

and experimental results including the mean f_{fu}, ε_{fu} and E_f. The stress-strain curves of the GFRP reinforcement bars were linear up to the point of rupture with no yielding. The design compressive strengths of the concrete mixes were 50 MPa and 70 MPa. Three cylinders from each concrete batch were tested to determine the compressive strengths of concrete. The concrete cylinders tested were 100 mm in diameter and 200 mm in height. The average compressive strengths of concrete of the three cylinders tested were 47 MPa and 66 MPa at 28 days.

3.2 *Details of GFRP-RC beams*

Eight GFRP-RC beams were constructed with 100 mm in width, 150 mm in height, 2400 mm in length, and 15 mm clear concrete cover as shown in Figure 3. The GFRP-RC beams were all tested under static loading until failure. Six beams were tested under four-point bending and two beams under three-point bending. The main test variables were the FRP reinforcement ratios and the compressive strengths of concrete. Three different diameters of FRP bars were used: 6.35 mm (#2), 9.53 mm (#3) and 12.7 mm (#4), providing reinforcement ratios of $\rho_f = 0.5\%, 1\%,$ and 2%, respectively. Two GFRP reinforcement bars were used in compression (to hold the shear reinforcement and to form the reinforcement cage) and two similar bars were used in tension. The 4 mm diameter steel stirrups at 100 mm centres were used as shear reinforcement, as shown in Figure 3b. The experimental setup of these beams was shown in Figure 4a and Figure 4b. The loads and midspan deflections were measured using a load cell and a linear potentiometer, respectively. One strain gauge was attached to one GFRP bar in tension of each beam at the midspan and another strain gauge was attached to the surface of concrete at the compression zone at the midspan of the beam. In the three-point bending configuration, the load was applied at the midspan of the beam, whereas in the four-point bending configuration, the load was applied at a distance of 667 mm ($L/3$) from the supports.

The GFRP-RC beams were analysed in accordance with ACI [24] and CSA [25] to compare with experimental data. The GFRP-RC beams were designed for three failure modes. One GFRP-RC beam was designed as a balanced beam, one GFRP-RC beam was designed as an under-reinforced beam, and the remaining six GFRP-RC beams were designed as over-reinforced beams.

The GFRP-RC beams were labelled (Table 3) in the form A-B-C. The first number (A) represents the design compressive strength of concrete (47 MPa or 66 MPa), the second number (B) represents the percentage of the reinforcement ratio (0.5%, 1%, or 2%), and the third number (C) represents the condition of loading (3 for three-point bending or 4 for four-point bending). For example, Beam 47-0.5-4 represents the GFRP-RC beam constructed with concrete compressive strength of 47 MPa, reinforcement ratio of $\rho_f = 0.5\%$ and tested under four-point bending. Table 3 presents the experimental maximum load (P_{exp}), midspan deflection at the maximum load $\left(\Delta_{exp}\right)$, and Energy Absorption Capacity $\left(EAC_{exp}\right)$ of the tested GFRP-RC beams. The maximum load was defined as the load corresponding to the first major drop in the load for the over-reinforced GFRP-RC beams or failure of the balanced and under-reinforced GFRP-RC beams. The data reported in Table 3 was calculated using the material data obtained from preliminary material testing. The maximum load $\left(P_{exp}\right)$ was calculated for four-point bending ($P_{exp} = 6M_n/L$) and for three-point bending ($P_{n,exp} = 4M_n/L$) as well, where L was the clear span length of the beam ($L = 2000$ mm). All the GFRP-RC beams were designed to fail in flexure.

4. Experimental results and discussion

Initially, all eight GFRP beams displayed high bending stiffness ($E_c I_g$). However, once cracking initiated, the stiffness of the beam decreased due to the contribution of GFRP bars with a low modulus of elasticity. The cracking load was recorded as the load where the first crack in concrete was observed. The change from the pre-cracking bending stiffness ($E_c I_g$) to the post-cracking bending stiffness (E_cI_e) was shown in Figure 5. For example, in case of the GFRP-RC Beam 47-0.5-4, with a reinforcement ratio of 0.5%, the post-bending stiffness (E_cI_e) was 8% of the pre-cracking bending stiffness (E_cI_g). Also, the GFRP-RC beams with higher reinforcement ratio ($\rho_f = 1.0\%$ and 2.0%) had higher post-cracking bending stiffness due to the higher modulus of elasticity of the #3 and #4 GFRP bars. Hence, GFRP-RC beams with a higher elastic modulus of the GFRP bars have comparatively higher post-cracking bending stiffness.

For the two GFRP-RC beams with the same reinforcement ratio ($\rho_f = 0.5\%$) but different compressive strengths of concrete (47 MPa and 66 MPa), it was observed that the post-cracking bending stiffness (E_cI_e) increased by 7% (from Beam 47-0.5-4 to Beam 66-0.5-4) when the compressive strength of concrete increased from 47 MPa to 66 MPa. On the other hand, for Beam 47-0.5-4 and Beam 47-1.0-4, with the same compressive strength of concrete but different reinforcement ratios, it was observed that the post-cracking bending stiffness (E_cI_e) increased with the increase in the reinforcement ratio. The post-cracking bending stiffness of Beam 47-1.0-4 was 1.8 times the post-cracking bending stiffness of Beam 47-0.5-4. This means that the post-cracking bending stiffness of the GFRP-RC beam was influenced by the reinforcement ratio more than it was influenced by the compressive strength of concrete.

The ${\rho_f}/{\rho_{fb}}$ ratio was calculated according to ACI [24] for all the beams tested and was presented in Table 3 to determine whether the beams were under-reinforced, balanced, or over-reinforced. The under-reinforced GFRP-RC Beam 66-0.5-4 with $\rho_f = 0.5\%$ failed once the maximum load (P_{exp}) was reached. There was no warning prior to the collapse of the beam with the rupture of the GFRP bars. Figure 6 shows the failure mode of Beam 66-0.5-4 due to GFRP bar rupture. Moreover, for the balanced GFRP-RC beams (Beams 47-0.5-4 and 47-0.5-3), crushing of the concrete cover and GFRP bar rupture occurred simultaneously at the point of failure, as shown in Figure 7 (only one beam was chosen for presentation purposes since both balanced GFRP-RC beams showed a similar failure mode). For the under-reinforced and balanced beams, the readings of the strain gauges at the compressive side of concrete (ε_c = 0.0014) were lower than ultimate strain values specified by the design codes (ε_{cu}= 0.003) which confirm the codes predictions. Furthermore, crushing of the concrete cover was the assumed failure for the six over-reinforced GFRP-RC beams, which occurred at the first drop in the load ($P_{n,exp}$). At the time of failure, all GFRP-RC beams displayed a flexural-critical response with vertical cracks initially propagating in the pure bending region before moving towards the supports. These cracks continued to extend through the depth of the GFRP-RC beams towards the compression zone, as shown in Figure 8 for Beam 47-1.0-4. The over reinforced GFRP-RC beams continued to sustain load after the first drop in the maximum load (Figure 9), indicating a sign of pseudo "ductility" or reserve capacity. The readings of the strain gauges at the failure of the beams were in the vicinity of 0.003, ranging between 0.0027 and 0.0033 and having a mean value of 0.0029. The load-midspan deflection curves of an under-reinforced, balanced, and over-reinforced GFRP-RC beam were presented in Figure 9. It can be observed from Figure 9 that the ACI [24] and CSA [25] load-midspan deflection curves reasonably matched with the experimental load-midspan deflection curves. The initial pre-cracked behaviour of the beam was captured by both ACI [24] and CSA [25]. The ACI [24] and CSA [25] also captured the slope of the post-cracking bending stiffness. The ACI [24] showed a bilinear response of the load-midspan deflection at the nominal load of the GFRP-RC beams, whereas CSA [25] showed a trilinear response of the load-midspan deflection at the nominal load of the GFRP-RC beams. Table 3 provides a summary of the experimental results including the maximum load $\left(P_{exp}\right)$ defined as the load corresponding to the first major drop in the load for the over-reinforced GFRP-RC beams or failure of the balanced and under-reinforced GFRP-RC beams (Figure 9). Moreover, Table 3 provides the midspan deflections (Δ_{exp}) at the maximum loads $\left(P_{exp}\right)$ and the Energy Absorption Capacities (EAC_{exp}) of the beams. Adhikary et al. [28-29] used the term Energy Absorption Capacity (EAC) to define the energy absorbed by the beam and calculated it as the area under the load-midspan deflection curve. In other words, the EAC was the integral of the load–midspan deflection graph from zero to the midspan deflection corresponding to the maximum load $\left(\int_0^{\Delta_{exp}} P.\,d\Delta\right)$, where Δ_{exp} was the midspan deflection corresponding to the maximum load. It was noted from Table 3 that as the reinforcement ratio increased, the maximum load (P_{exp}) of the GFRP-RC beams increased as well. The maximum loads for the GFRP-RC beams with 1% reinforcement ratio for Beams 47-1.0-4 and 66-1.0-4 were 39.18 kN and 42.65 kN respectively. Upon increasing the reinforcement ratio to 2%, the maximum loads increased to 49.7 kN and 49.53 kN for Beams 47-2.0-4 and 66-2.0-4, respectively. The increase in the maximum loads was 27% and 16% for the increase of the reinforcement ratio from 1% to 2%. However, for the increase of the reinforcement ratio from 0.5% to 1%, the increase in the maximum load was significantly larger. Beams 47-0.5-4 and 66-0.5-4 had maximum loads of 13.7 kN and 15.52 kN, respectively, whereas Beams 47-1.0-4 and 66-1.0-4 had maximum loads of 39.18 kN and 42.65 kN, respectively. The increase in the maximum loads (186% and 175%) for beams with a reinforcement ratio of 0.5% compared to beams with a reinforcement ratio of 1% was significantly larger than the increase in the maximum loads for beams with a reinforcement ratio of 1% compared to beams with a reinforcement ratio of 2%. This increase was due to the shift in the failure mode from under-reinforced and balanced failure modes to over-reinforced failure mode. The GFRP-RC beams that were designed to fail due to GFRP bar rupture resisted a maximum load that was significantly less than that of the GFRP-RC beams that were designed to fail due to concrete crushing. Moreover, the influence of the compressive strength of concrete on the maximum loads of the beams was investigated. Beams with similar reinforcement ratio but different compressive strengths of concrete (47 MPa and 66 MPa) were analysed. It was found that an increase in the compressive strength of concrete for beams with a fixed reinforcement ratio of 0.5% (Beams 47-0.5-4 and 66-0.5-4) experienced an increase in the maximum load by 13%.

5. Experimental results versus recommendations in FRP design codes

The experimental results obtained from the testing of GFRP-RC beams under four-point and three-point bending were compared with the FRP design recommendations in ACI [24] and CSA [25] in terms of the failure mode, nominal load, midspan deflection at the nominal load, and Energy Absorption Capacity (EAC). Table 3 presents the experimental and code predictions, in ACI [24] and CSA [25], of the maximum and nominal loads $\left(P_{exp}, P_{n,ACI}, P_{n,CSA}\right)$, midspan deflections at maximum and nominal loads $\left(\Delta_{exp}, \Delta_{n,ACI}, \Delta_{n,CSA}\right)$, and EAC $\left(EAC_{exp}, EAC_{n,ACI}, EAC_{n,CSA}\right)$ of the GFRP-RC beams. The calculations of the reinforcement ratios, nominal loads, midspan deflections at nominal loads, and EAC in ACI [24] and CSA [25] were based on the data obtained from the preliminary material testing. It is noted that the stress block parameters used in this manuscript were based on the recommendations in ACI [24] and CSA [25]. Table 4 presents the comparisons between the experimental results and the code predictions from ACI [24] and CSA [25]. The results were presented in terms of the difference (in percent) between the experimental results and the predictions of ACI [24] and CSA [25]. The positive numbers indicate that the design codes under-predict the behaviour, whereas the negative numbers indicate that the design codes over-predicted the results.

The ACI [24] and CSA [25] accurately predicted the failure modes of GFRP-RC beams. Beam 47-0.5-4 with a reinforcement ratio $\left({}^{\rho_f}/_{\rho_{fb}}\right)$ of 1.02 (calculated as per ACI [24], where 1.02 was between 1 and 1.4) was balanced and failed due to simultaneous rupture of the GFRP bars and concrete crushing. Beam 66-0.5-4 with a reinforcement ratio $\left({}^{\rho_f}/_{\rho_{fb}}\right)$ of 0.7 (less than 1) failed due to GFRP bar rupture. The remaining over-reinforced beams with reinforcement ratios $\left({\rho_f}/{\rho_{fb}}\right)$ higher than 1.4 failed due to concrete crushing on the compression side.

5.1 *Influence of the reinforcement ratio of GFRP-RC beam*

The under-reinforced Beam 66-0.5-4 failed at a maximum load of 15.5 kN (Figure 10 (a)) and a midspan deflection at the maximum load of 54.53 mm, Figure 10 (b). The EAC was calculated to be 518.2 J under four-point bending, Figure 10 (c). The predictions of the nominal load, midspan deflection at the nominal load, and EAC were 17.2 kN, 59 mm, and 660.36 J, respectively, according to ACI [24]. The predictions of the nominal load, midspan deflection at the nominal load, and EAC were 16.5 kN, 64.2 mm, and 644.67 J, respectively, according to CSA [25]. The ACI [24] over-predicted the maximum load, midspan deflection at the maximum load, and EAC by 10%, 8%, and 22%, respectively, whereas CSA [25] over-predicted the maximum load, midspan deflection at the maximum load, and EAC by 6%, 15%, and 20%, respectively. Hence, both ACI [24] and CSA [25] over-predicted the response of the under-reinforced GFRP-RC beam.

The balanced Beam 47-0.5-4 failed at a maximum load of 13.7 kN and a midspan deflection at the maximum load of 52.2 mm. The EAC was calculated to be 433.74 J under four-point bending. The ACI [24] over-predicted the maximum load, midspan deflection at the maximum load, and EAC by 20%, 15%, and 35%, respectively. The CSA [25] over-predicted the maximum load, midspan deflection at the maximum load, and EAC by 17%, 21%, and 32%, respectively. Hence, both ACI [24] and CSA [25] over-predicted the response of the balanced GFRP-RC beams.

For the over-reinforced beams both ACI [24] and CSA [25] under-predicted the response of all six over-reinforced GFRP-RC beams in terms of the maximum loads, midspan deflections at maximum loads, and EAC. The ACI [24] under-predicted the average maximum loads, midspan deflections at maximum loads, and EAC of the six over-reinforced GFRP-RC by 38%, 41%, and 65%, respectively. Whereas, the CSA [25] under-predicted the average maximum loads, midspan deflections at maximum loads, and EAC of the six beams by 27%, 33%, and 52%, respectively. Hence, both codes under-predicted the response of the over-reinforced GFRP-RC beams.

In general, ACI [24] predicted higher nominal loads and EAC than CSA [25], while ACI [24] predicted lower deflections than CSA [25]. Moreover, for the under-reinforced and balanced beams, ACI [24] predicted midspan deflections at nominal loads closer to the experimental results. However, CSA [25] predicted nominal loads and EAC that were closer to the experimental results. For the over-reinforced GFRP-RC beams, it can be observed from Table 3 that ACI [24] predicted higher nominal loads, midspan deflections at nominal loads, and EAC than CSA [25] $\left(P_{n,ACI} > P_{n,CSA},\ \Delta_{n,ACI} > \Delta_{n,CSA}\right.$ and $\left.EAC_{n,ACI} > EAC_{n,CSA}\right)$. The ACI [24] predicted higher nominal loads, midspan deflections at nominal loads, and EAC by an average of 27%, 20%, and 43%, respectively than CSA [25]. This means that CSA [25] was more conservative than the ACI [24] in terms of predicting the nominal loads, midspan deflections at nominal loads, and EAC.

5.2 *Influence of the tensile reinforcement ratio of the GFRP-RC beam*

It was observed that both ACI [24] and CSA [25] predicted responses of the GFRP-RC beams closer to the experimental results in terms of the maximum loads, midspan deflections at maximum loads, and EAC for a reinforcement ratio of 1% than for a reinforcement ratio of 2%. For example, for Beam 66-1.0-3 with a reinforcement ratio of 1%, the experimental maximum load was 32.9 kN. The predicted nominal loads from ACI [24] and CSA [25] were 23.5 kN and 19.2 kN, respectively. The ACI [24] and CSA [25] under-predicted the maximum load by 29% and 42%, respectively. On the other hand, for beams with 2% reinforcement ratio such as Beam 66-2.0-3, the experimental maximum load was 46.1 kN. The predictions from ACI [24] and

CSA [25] were 27.6 kN and 22.9 kN, respectively. The ACI [24] and CSA [25] under-predicted the maximum load by 40% and 50%, respectively. For example, ACI [24] and CSA [25] predicted the response of Beam 66-1.0-4 closer to the experimental results than Beam 66-2.0-3 in terms of the maximum load, midspan deflection at the maximum load, and EAC. Hence, the predictions of the ACI [24] and CSA [25] were closer to the experimental results for a reinforcement ratio of 1% than for a reinforcement ratio of 0.5% and 2%.

5.3 *Influence of the compressive strength of concrete of the GFRP-RC beam*

It was observed that both design guidelines predicted the response of the GFRP-RC beams closer to the experimental results in terms of the maximum loads, midspan deflections at maximum loads, and EAC for beams with a higher compressive strength of concrete. For example, Beam 47-2.0-4 had a midspan deflection at the maximum load of 59.9 mm. The predicted midspan deflections at nominal loads by the ACI [24] and CSA [25] for Beam 47-2.0-4 were 33.9 mm and 31.2 mm, respectively. The ACI [24] and CSA [25] under-predicted the midspan deflections at maximum loads by 43% and 48%, respectively. On the other hand, Beam 66-2.0-4 had a midspan deflection at the maximum load of 47.3 mm. The midspan deflections at nominal loads predicted by ACI [24] and CSA [25] were 38.94 mm and 33.67 mm, respectively. The ACI [24] and CSA [25] under-predicted the midspan deflections at nominal loads values by 18% and 29%, respectively. The predictions were closer for GFRP-RC beams with the compressive strength of concrete of 66 MPa than for GFRP-RC beams with the compressive strength of concrete of 47 MPa. The same was observed for the nominal loads and EAC where the predictions of the ACI [24] and CSA [25] were closer to the experimental results in the case of beams with a compressive strength of concrete of 66 MPa than beams with a compressive strength of concrete of 47 MPa. Hence, the predictions of the design guidelines were closer to the experimental results for the GFRP-RC beams with a higher compressive strength of concrete.

6. Conclusions

In this study, eight GFRP-RC beams were tested under static loads. The experimental load-deformation relationships and Energy Absorption Capacities (EAC) were measured and analysed. The flexural design of the GFRP-RC beams according to the ACI [24] and CSA [25] was presented. Comparisons between the experimental data and predictions of ACI [24] and CSA [25] were presented. Based on the results of the experimental and analytical investigations, the following conclusions are drawn:

1. The failure modes of GFRP-RC beams were accurately predicted by the sectional analysis techniques used for GFRP-RC beams. The ρ_f/ρ_{fb} ratio held true for the failure mode of all the GFRP-RC beams. The GFRP-RC beams designed as over-reinforced ($\rho_f/\rho_{fb} > 1.4$) failed due to the crushing of concrete. The under-reinforced GFRP-RC beams ($\rho_f/\rho_{fb} < 1$) failed by the rupture of the tensile GFRP bars. The balanced GFRP-RC beams ($1 < \rho_f/\rho_{fb} < 1.4$) failed by the simultaneous crushing of concrete cover and rupture of GFRP bars.
2. The response of the GFRP-RC beams was found to depend on the reinforcement ratio and concrete strength. It was found that increasing the GFRP reinforcement ratio increased the maximum loads of the GFRP-RC beams, regardless of the concrete strength. An increase in the maximum loads by an average of 22% was observed when the reinforcement ratio of the beam was increased from $\rho_f = 1\%$ to $\rho_f = 2\%$. However, a significant increase in the maximum load was observed when the reinforcement ratio was increased from $\rho_f = 0.5\%$ to $\rho_f = 1\%$. The maximum load increased by an average of 180% when reinforcement ratio increased from $\rho_f = 0.5\%$ to $\rho_f = 1.0\%$. This was because the failure mode changed from GFRP reinforcement rupture $\left(\text{in case of } \rho_f = 0.5\%\right)$ to concrete crushing $\left(\text{in case of } \rho_f = 1\%\right)$. However, it was found that the compressive strength of concrete has less significant influence than the reinforcement ratio on the response of GFRP-RC beams.

3. Design recommendations for GFRP-RC beams provided in ACI [24] and CSA [25] were found to be conservative and under-predicted the response of the GFRP-RC beams in terms of the maximum loads, midspan deflections at maximum loads, and EAC for the over-reinforced beams. Whereas, these guidelines over-predicted the response of the under-reinforced and balanced GFRP-RC beams. On average, for over-reinforced GFRP-RC beams, CSA [25] under-predicted the maximum load, midspan deflection at the maximum load, and EAC by 38%, 41%, and 65%, respectively, whereas ACI [24] under-predicted the maximum load, midspan deflection at maximum load, and EAC by 27%, 33%, and 52%, respectively. As for GFRP-RC beams failing due to GFRP bar rupture (including both under-reinforced and balanced), CSA [25] over-predicted the maximum load, midspan deflection at the maximum load, and EAC by 11%, 18%, and 26% respectively, whereas ACI [24] over-predicted maximum load, midspan deflection at the maximum load, and EAC by 15%, 11%, and 28% respectively.

4. The ACI [24] predicted higher nominal loads, midspan deflections at nominal loads, and EAC than CSA [25] by a range between 20% and 43%. The CSA [25] was more conservative in the predictions of the nominal loads, midspan deflections at nominal loads, and EAC than ACI [24]. Moreover, ACI [24] predicted values that were closer to the experimental results than CSA [25].

5. Both ACI [24] and CSA [25] predicted closer results to the experimental results in terms of the maximum loads, midspan deflections at maximum loads, and EAC for GFRP-RC beams with high concrete compressive strength (66 MPa) and a reinforcement ratio of $\rho_f = 1.0\%$.

Acknowledgments

The authors wish to express their gratitude for the support received from the University of Wollongong in providing the funding and facilities for the experimental and numerical work presented in this paper.

References

[1] Boukhezar M, Samai M. L, Mesbah H. A, and Houari H, "Flexural behaviour of reinforced low-strength concrete beams strengthened with CFRP plates," *Structural Engineering and Mechanics,* vol. 47, no. 6, pp. 819-838, 2013.

[2] Huang, L., Yan, B., Yan, L., Xu, Q., Tan, H. and Kasal, B., "Reinforced concrete beams strengthened with externally bonded natural flax FRP plates," *Composites Part B: Engineering*, *91*, pp.569-578, 2016.

[3] Ghasemi S, Maghsoudi A. A, Bengar H. A, and Ronagh H. R, "Flexural strengthening of continuous unbonded post-tensioned concrete beams with end-anchored CFRP laminates," *Structural Engineering and Mechanics,* vol. 53, no. 6, pp. 1083-1104, 2015.

[4] Hadi MNS, "Comparative study of eccentrically loaded FRP wrapped columns," *Composite structures,* vol. 74, no. 2, pp. 127-135, 2006.

[5] Hadi MNS, "Behaviour of FRP strengthened concrete columns under eccentric compression loading," *Composite Structures,* vol. 77, no. 1, pp. 92-96, 2007.

[6] Kim M.S, Lee Y.H, Kim H, Scanlon A, and Lee J, "Flexural behavior of concrete beams reinforced with aramid fiber reinforced polymer (AFRP) bars," *Structural Engineering and Mechanics,* vol. 38, no. 4, pp. 459-477, 2011.

[7] Goldston M, Remennikov A, Sheikh MN, "Experimental investigation of the behaviour of concrete beams reinforced with GFRP bars under static and impact loading," *Engineering Structures,* vol. 113, pp. 220-232, 2016.

[8] Nakano K, Matsuzaki Y, Fukuyama H, and Teshigawara M, "Flexural performance of concrete beams reinforced with continuous fiber bars," *Special Publication,* vol. 138, pp. 743-766, 1993.

[9] Benmokrane B, Chaallal O, and Masmoudi R, "Flexural response of concrete beams reinforced with FRP reinforcing bars," *ACI Structural Journal,* vol. 93, no. 1, pp. 46-55, 1996. [10] Alsayed S , "Flexural behaviour of concrete beams reinforced with GFRP bars," *Cement and Concrete Composites,* vol. 20, no. 1, pp. 1-11, 1998.

[10] Alsayed S , "Flexural behaviour of concrete beams reinforced with GFRP bars," *Cement and Concrete Composites,* vol. 20, no. 1, pp. 1-11, 1998.

[11] Alsayed S, Al-Salloum Y, and Almusallam T, "Performance of glass fiber reinforced plastic bars as a reinforcing material for concrete structures," *Composites Part B: Engineering,* vol. 31, no. 6, pp. 555-567, 2000.

[12] Toutanji HA and Saafi M, "Flexural behavior of concrete beams reinforced with glass fiber-reinforced polymer (GFRP) bars," *ACI Structural Journal,* vol. 97, no. 5, pp. 712-719, 2000.

[13] Sam A.R.M. and Swamy R.N, "Flexural behaviour of concrete beams reinforced with glass fibre reinforced polymer bars," *Malaysian Journal of Civil Engineering,* vol. 17, no. 1, pp. 49-57, 2005.

[14] Ashour A, "Flexural and shear capacities of concrete beams reinforced with GFRP bars," *Construction and Building Materials,* vol. 20, no. 10, pp. 1005-1015, 2006.

[15] Yazici V, Hadi MN. Axial load-bending moment diagrams of carbon FRP wrapped hollow core reinforced concrete columns. J Compos Constr. 2009;13:262-8.

[16] Adam M.A, Said M, Mahmoud A.A, and Shanour A.S, "Analytical and experimental flexural behavior of concrete beams reinforced with glass fiber reinforced polymers bars," *Construction and Building Materials,* vol. 84, pp. 354-366, 6/1/ 2015.

[17] Wang W, Sheikh MN, Hadi MN. Experimental study on FRP tube reinforced concrete columns under different loading conditions. J Compos Constr. 2016;20:04016034.

[18] Hadi MN, Hasan HA, Sheikh MN. Experimental investigation of circular high-strength concrete columns reinforced with glass fiber-reinforced polymer bars and helices under different loading conditions. J Compos Constr. 2017;21:04017005.

[19] Wang W, Sheikh MN, Hadi MN, Gao D, Chen G. Behaviour of concrete-encased concrete-filled FRP tube (CCFT) columns under axial compression. Engineering Structures. 2017;147:256-68.

[20] Hasan HA, Sheikh MN, Hadi MN. Analytical investigation on the load-moment characteristics of GFRP bar reinforced circular NSC and HSC columns. Construction and Building Materials. 2018;183:605-17.

[21] Goldston M, Remennikov A, Sheikh M.N, "Flexural behaviour of GFRP reinforced high strength and ultra high strength concrete beams," *Construction and Building Materials,* vol. 131, pp. 606-617, 2017.

[22] Kalpana V.G. and Subramanian K, "Behavior of concrete beams reinforced with GFRP BARS," *Journal of Reinforced Plastics and Composites,* vol. 30, no. 23, pp. 1915-1922, 2011.

[23] Gravina R.J and Smith S.T, "Flexural behaviour of indeterminate concrete beams reinforced with FRP bars," *Engineering Structures,* Article vol. 30, no. 9, pp. 2370-2380, 2008.

[24] ACI, "Guide for the Design and Construction of Structural Concrete Reinforced with Fiber-Reinofrced Polymer (FRP) Bars (ACI 440.1R-15)," *American Concrete Institute,* Detroit, Michigan, 2015.

[25] CSA, Design and construction of building structures with fibre-reinforced polymers. *Canadian Standards Association*, 2012.

[26] CNR, "Guide for the design and construction of concrete structures reinforced with fiber-reinforced polymer bars," *National Research Council (CNR), CNR-DT 203/2006,* 2006.

[27] ISIS, "Reinforcing concrete structures with fibre reinforced polymers (FRPs). Design Manual 3 " *ISIS-M03-01, The Canadian Network of Centres of Excellence on Intelligent Sensing for Innovative Structures,* ISIS Canada, University of Manitoba, Winnipeg, Man, 2007.

[28] Machida A and Uomoto T, "Recommendation for design and construction of concrete structures using continuous fiber reinforcing materials," *Japan Soc. of Civil Engineers*, 1997.

[29] A. D. D7205M-06, "Standard Test Method for Tensile Properties of Fiber Reinforced Polymer Matrix Composite Bars," *ASTM International,* West Conshohocken, PA, 2016.

[30] Hadi M.N.S, Karim H, Sheikh M.N, "Experimental Investigations on Circular Concrete Columns Reinforced with GFRP Bars and Helices under Different Loading Conditions," *J Compos Constr*, vol. 20, pp. 04016009, 2016.

[31] Hasan H.A, Sheikh M.N, Hadi M.N.S, "Performance evaluation of high strength concrete and steel fibre high strength concrete columns reinforced with GFRP bars and helices," *Construction and Building Materials*, vol. 134, pp. 297-310, 2017.

[32] Adhikary S.D, Li B, Fujikake K, "Dynamic behavior of reinforced concrete beams under varying rates of concentrated loading," *International Journal of Impact Engineering*, vol. 47, pp. 24-38, 2012.

[33] Adhikary S.D, Li B, Fujikake K, "Residual resistance of impact-damaged reinforced concrete beams," *Magazine of Concrete Research*, vol **67,** no.7, pp. 364-378, 2015.

List of tables

Table 1 Nominal tensile properties of the reinforcing bars (ACI [24])

Table 2 Results of tested GFRP bars

Table 3 Maximum load, midspan deflection at maximum load, EAC, and shear capacity of the GFRP-RC beams tested

Table 4 Experimental results versus the predictions from ACI [24] and CSA [25]

List of figures

Figure 1. Stress-strain behaviour of reinforcement bars based on average values taken from ACI [24]

Figure 2. Strength reduction factor as a function of the reinforcement ratio (ACI [24])

Figure 3. Details of the tested GFRP-RC beams: (a) Cross-sectional view (b) Side view

Figure 4. Testing of the GFRP-RC beams:(a) Four-point bending and (b) Three-point bending

Figure 5. Load-midspan deflection behaviour of GFRP-RC Beams

Figure 6. Rupture of GFRP reinforcement bars (Beam 66-0.5-4)

Figure 7. Balanced Failure (Beam 47-0.5-4)

Figure 8. Flexural response with crushing of concrete cover (47-1.0-4)

Figure 9. Load-midspan deflection behaviour: (a) under-reinforced (66-0.5-4), (b) balanced (47-0.5-4), and (c) over-reinforced (47-2.0-4) GFRP-RC beams

Figure 10. Experimental results and design code predictions of Beam 66-0.5-4

Table 1 Nominal tensile properties of the reinforcing bars (ACI [24])

Material properties	GFRP	CFRP	AFRP	Steel
Tensile strength (MPa)	483-1600	600-3690	1720-2540	483-690
Elastic modulus (GPa)	35-51	120-580	41-125	200
Rupture strain (%)	1.2-3.1	0.5-1.7	1.9-4.4	6-12

Table 2 Results of tested GFRP bars

Specimen	L_a (mm)	L (mm)	L_{tot} (mm)	f_u (MPa)	ε_{fu} (%)	E_f (GPa)
6.35 mm (#2)	150	380	680	732	1.96	37.5
9.53 mm (#3)	400	200	1000	1764	3.18	55.6
12.7 mm (#4)	400	200	1000	1605	3.30	48.6

Table 3 Maximum load, midspan deflection at maximum load, EAC, and shear capacity of the GFRP-RC beams tested

Beam	ρ_f / ρ_{fb}		Experimental			ACI [24]			CSA [25]		
	CSA [25]	ACI [24]	P_{exp} (kN)	Δ_{exp} (mm)	EAC_{nxp} (J)	$P_{n,ACI}$ (kN)	$\Delta_{n,ACI}$ (mm)	$EAC_{n,ACI}$ (J)	$P_{n,CSA}$ (kN)	$\Delta_{n,CSA}$ (mm)	$EAC_{n,CSA}$ (J)
47-0.5-4	0.91	1.02	13.7	52.2	433.74	17.20	61.61	662.96	16.5	66.4	635.6
47-1-4	6.53	7.56	39.18	60.39	1370.89	29.60	40.90	680.07	26.1	37.2	521.27
47-2-4	11.1	12.8	49.7	59.9	1788.95	34.50	33.93	641.08	30.9	31.15	507.13
66-0.5-4	0.66	0.7	15.52	54.53	518.2	17.20	59.02	660.36	16.5	64.23	644.67
66-1-4	5.56	5.94	42.65	56.33	1347.23	34.50	46.87	903.49	28.9	40.6	630.9
66-2-4	9.42	10.1	49.53	47.3	1290.3	40.30	38.94	857.35	34.3	33.67	612.64
66-1-3	5.56	5.94	32.91	62.38	1230.77	23.50	36.70	489.89	19.2	31.82	330.2
66-2-3	9.42	10.1	46.14	58.34	1496.12	27.60	30.53	465.87	22.9	25.81	317.01

Table 4 Experimental results versus the predictions from ACI [24] and CSA [25]

Beam	ACI [24]			CSA [25]		
	$P_{exp} : P_{n,ACI}$ (%)	$\Delta_{exp}:\Delta_{n,ACI}$ (%)	$EAC_{exp}:EAC_{n,ACI}$ (%)	$P_{exp} : P_{n,CSA}$ (%)	$\Delta_{exp}:\Delta_{n,CSA}$ (%)	$EAC_{exp}:EAC_{n,CSA}$ (%)
47-0.5-4	-20	-15	-35	-17	-21	-32
47-1.0-4	24	32	50	33	38	62
47-2.0-4	31	43	64	38	48	72
66-0.5-4	-10	-8	-22	-6	-15	-20
66-1.0-4	19	17	33	32	28	53
66-2.0-4	19	18	34	31	29	53
66-1.0-3	29	41	60	42	49	73
66-2.0-3	40	48	69	50	56	79

Note: P_{exp} is the maximum load defined as the peak load at the first drop in the load-midspan deflection curves and Δ_{exp} is the midspan deflection at the maximum load

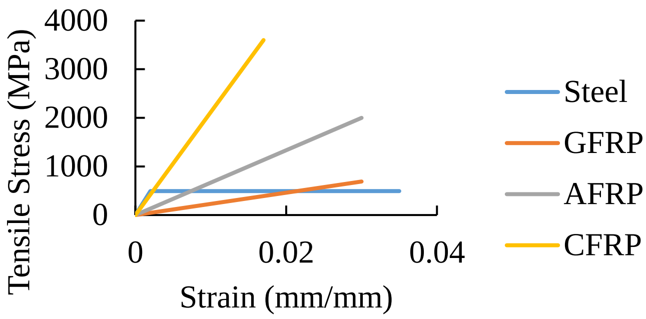

Figure 1. Stress-strain behaviour of reinforcement bars based on average values taken from ACI [24]

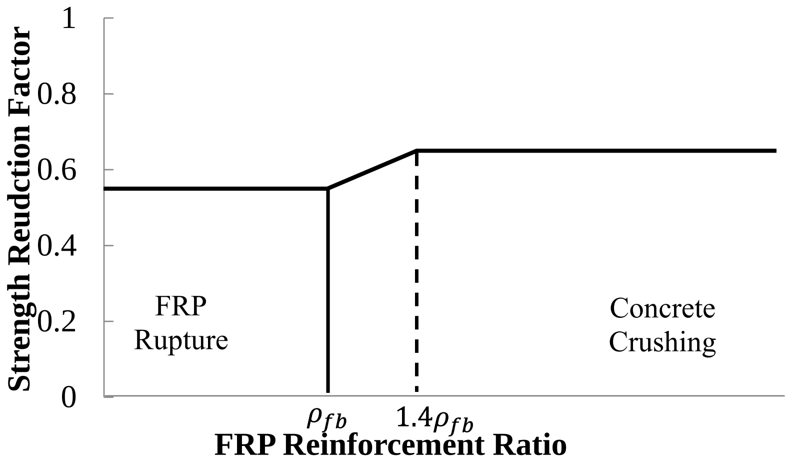

Figure 2. Strength reduction factor as a function of the reinforcement ratio (ACI [24])

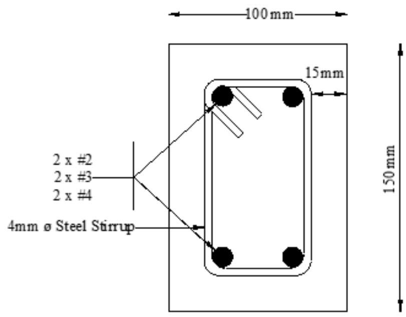

(a)

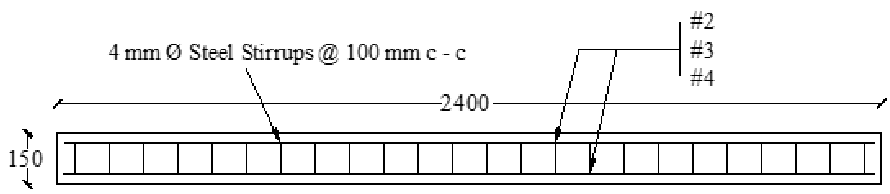

(b)

Figure 3. Details of the tested GFRP-RC beams: (a) Cross-sectional view (b) Side view

(a)

(b)

Figure 4. Testing of the GFRP-RC beams: (a) Four-point bending and (b) Three-point bending

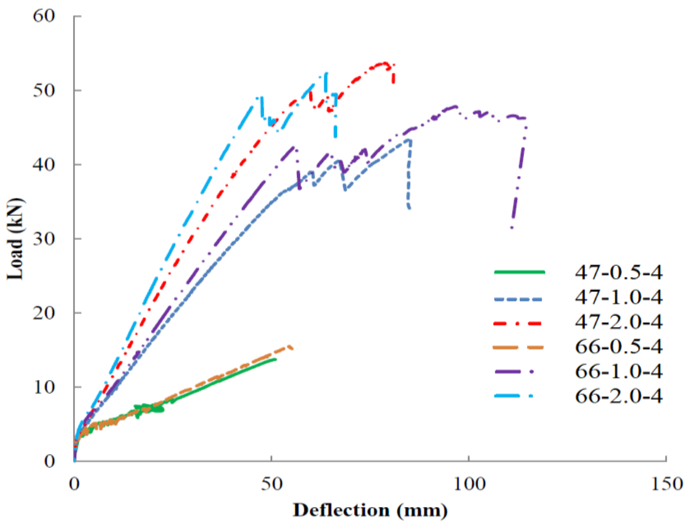

Figure 5. Load-midspan deflection behaviour of GFRP-RC Beams

Figure 6. Rupture of GFRP reinforcement bars (Beam 66-0.5-4)

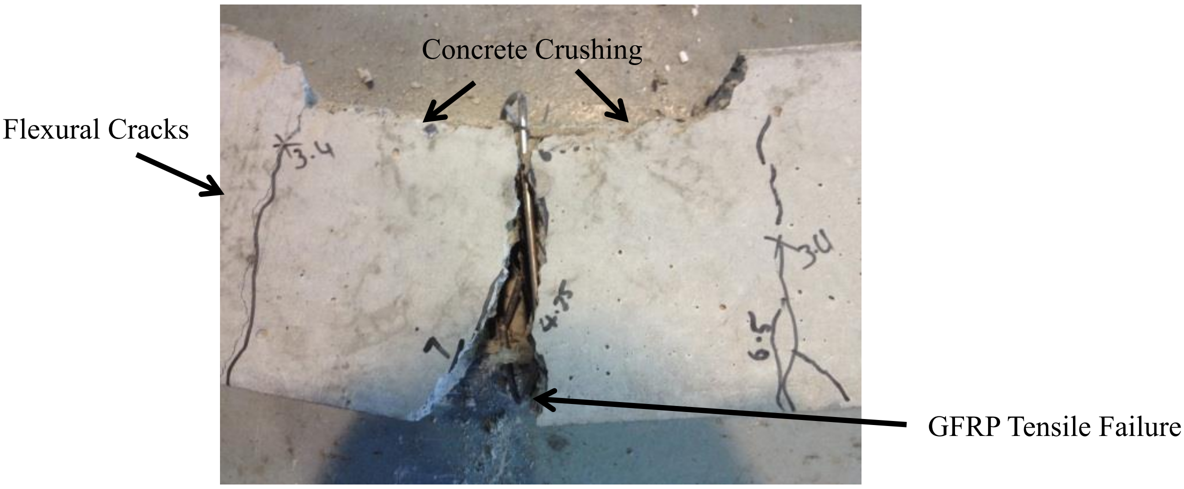

Figure 7. Balanced Failure (Beam 47-0.5-4)

Figure 8. Flexural response with crushing of concrete cover (47-1.0-4)

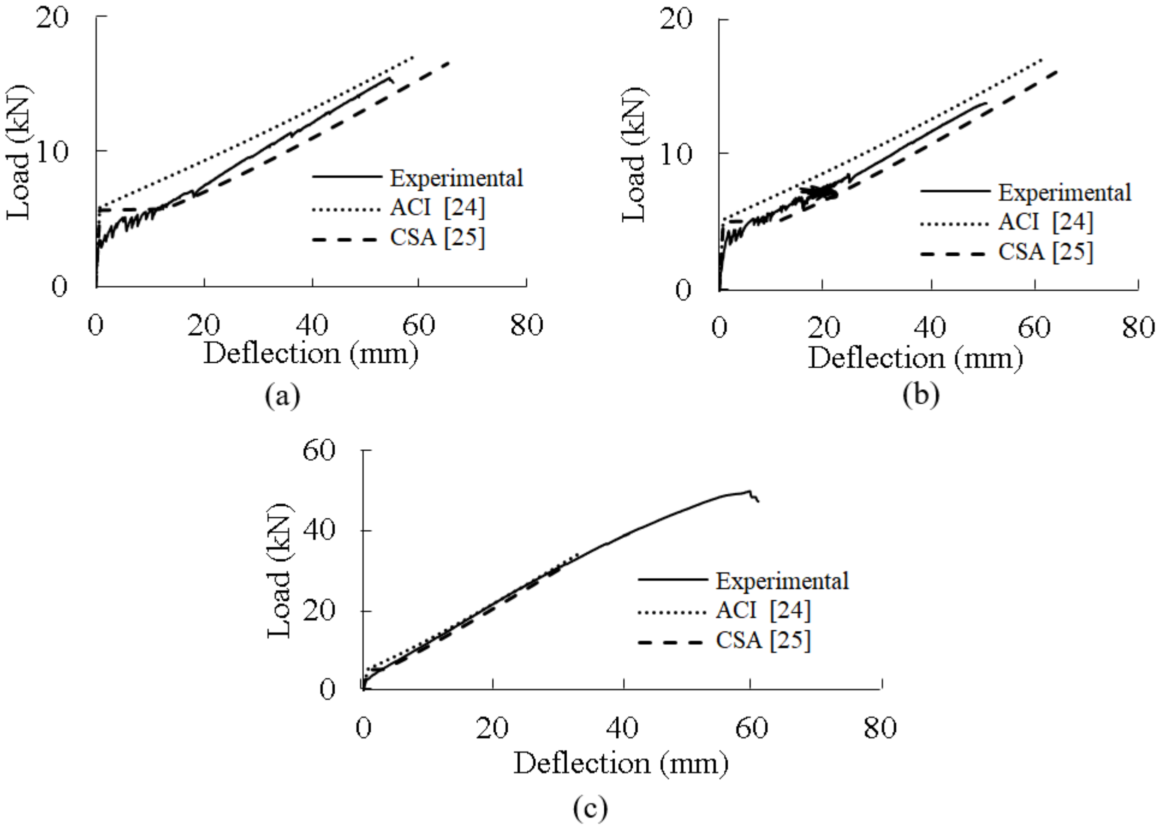

Figure 9. Load-midspan deflection behaviour: (a) under-reinforced (66-0.5-4), (b) balanced (47-0.5-4), and (c) over-reinforced (47-2.0-4) GFRP-RC beams

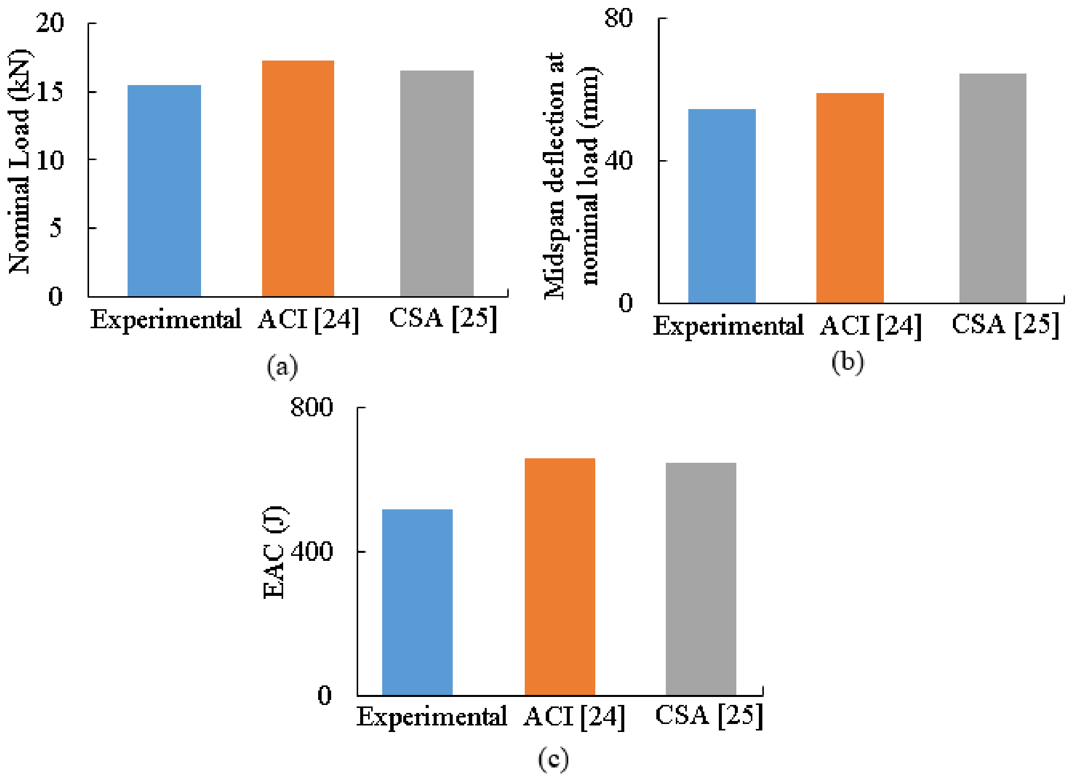

Figure 10. Experimental results and design code predictions of Beam 66-0.5-4